The Astrophysical Journal, 778:18 (9pp), 2013 November 20 doi:10.1088/0004-637X/778/1/18

THE SIGNATURE OF THE CENTRAL ENGINE IN THE WEAKEST RELATIVISTIC EXPLOSIONS: GRB 100316D

R. Margutti[1], A. M. Soderberg[1], M. H. Wieringa[2], P. G. Edwards[2], R. A. Chevalier[3], B. J. Morsony[4], R. Barniol Duran[5], L. Sironi[1], B. A. Zauderer[1], D. Milisavljevic[1], A. Kamble[1], and E. Pian[6,7]
[1] Harvard-Smithsonian Center for Astrophysics, 60 Garden Street, Cambridge, MA 02138, USA
[2] CSIRO Astronomy and Space Science, Australia Telescope National Facility, P.O. Box 76, Epping, NSW 1710, Australia
[3] Astronomy Department, University of Virginia, Charlottesville, VA 22904, USA
[4] Department of Astronomy, University of Wisconsin-Madison, 2535 Sterling Hall, 475 N. Charter Street, Madison, WI 53706-1582, USA
[5] Racah Institute for Physics, Edmund J. Safra Campus, Hebrew University of Jerusalem, Jerusalem 91904, Israel
[6] Scuola Normale Superiore, 7, I-56126 Pisa, Italy
[7] INAF-IASF Bologna, via Gobetti 101, I-40129 Bologna, Italy
Received 2013 August 7; accepted 2013 September 13; published 2013 October 29

ABSTRACT

We present late-time radio and X-ray observations of the nearby sub-energetic gamma-ray burst (GRB)100316D associated with supernova (SN) 2010bh. Our broad-band analysis constrains the explosion properties of GRB 100316D to be intermediate between highly relativistic, collimated GRBs and the spherical, ordinary hydrogen-stripped SNe. We find that $\sim 10^{49}$ erg is coupled to mildly relativistic ($\Gamma = 1.5$–2), quasi-spherical ejecta, expanding into a medium previously shaped by the progenitor mass-loss with a rate of $\dot{M} \sim 10^{-5}\ M_{\odot}\ \mathrm{yr}^{-1}$ (for an assumed wind density profile and wind velocity $v_w = 1000\,\mathrm{km\,s^{-1}}$). The kinetic energy profile of the ejecta argues for the presence of a central engine and identifies GRB 100316D as one of the weakest central-engine-driven explosions detected to date. Emission from the central engine is responsible for an excess of soft X-ray radiation that dominates over the standard afterglow at late times ($t > 10$ days). We connect this phenomenology with the birth of the most rapidly rotating magnetars. Alternatively, accretion onto a newly formed black hole might explain the excess of radiation. However, significant departure from the standard fall-back scenario is required.

Key words: gamma-ray burst: general – gamma-ray burst: individual (GRB 100316D)

Online-only material: color figures

1. INTRODUCTION

Gamma-ray bursts (GRBs; Klebesadel et al. 1973) are the most powerful stellar explosions in our universe, typically releasing $\sim 10^{51}$ erg (e.g., Frail et al. 2001) coupled to highly relativistic jets. Long GRBs, with a duration of the prompt γ-ray emission $\Delta t > 2$ s (Kouveliotou et al. 1993), are associated with the death of massive stars (see Hjorth & Bloom 2012 for a recent review) and give rise to the brightest displays. However, in the past few years, a new class of sub-energetic long GRBs has been recognized. (Soderberg et al. 2006a and references therein).

Sub-energetic GRBs appear to be quasi-spherical explosions energetically dominated by the non-relativistic ejecta that carry $\sim$99.9% of the explosion energy. Only $\sim$0.1% of the energy is coupled to mildly relativistic material. While the mildly relativistic ejecta clearly differentiate sub-energetic GRBs from ordinary hydrogen-stripped (Type Ib/c) supernovae (SNe; Soderberg et al. 2010b), their relativistic energy release is $\sim$100–1000 times lower than the typical 10^{51} erg of GRBs with fully relativistic outflows (Frail et al. 2001), and a factor $\sim 10^4$ lower than the most energetic GRBs (Cenko et al. 2011). The energy coupled with the slow, non-relativistic ejecta is, however, interestingly similar between ordinary and sub-energetic GRBs and comparable to the most energetic Type Ib/c SNe (e.g., Cano 2013). Sub-energetic GRBs therefore represent an intermediate class of explosions, bridging the gap between the highly relativistic, collimated GRBs and the more common Type Ib/c SNe.

Only a handful of sub-energetic GRBs have been discovered to date, including the nearby GRBs 980425 (e.g., Galama et al. 1998; Kulkarni et al. 1998), 031203 (Soderberg et al. 2004; Malesani et al. 2004), and 060218 (e.g., Soderberg et al. 2006a; Campana et al. 2006; Pian et al. 2006; Mazzali et al. 2006). While the intrinsic faintness limited their detection to the local universe, the rate per unit volume of sub-energetic GRBs indicates that they are $\sim$10 times more common than cosmological GRBs (Soderberg et al. 2006a; Cobb et al. 2006; Guetta & Della Valle 2007; Soderberg et al. 2010b), which led some authors to conclude that ordinary and sub-energetic GRBs have different origins (e.g., Liang et al. 2007; Virgili et al. 2009; Bromberg et al. 2011). Recent simulations of jet-driven stellar explosions instead pointed to the possibility that the observed rates of events might reflect the distribution of the duration of the central engine activity that powers the jet (Lazzati et al. 2012). Ordinary GRBs would be produced by the longer-lasting engines able to launch successful jets, while sub-energetic GRBs would result from "failed" jets that barely pierce through the stellar surface, thus connecting ordinary and sub-energetic GRBs to the same "family" of explosions. The origin of sub-energetic GRBs and their connection to both ordinary Type Ib/c SNe and highly relativistic GRBs is still an open issue.

More recently, the *Swift* satellite (Gehrels et al. 2004) added two new bursts to the sub-energetic class: GRBs 100316D (Starling et al. 2011; Fan et al. 2011) and 120422A (Zhang et al. 2012; Melandri et al. 2012; B. A. Zauderer et al., in preparation). The nearby ($z = 0.0593$; Chornock et al. 2010) GRB 100316D triggered *Swift* on 2010 March 16 at 12:44:50 UT, which we use as the explosion date throughout the paper. The smooth, long ($\Delta t > 1300$ s) and soft (spectral peak energy $E_{\rm pk} \sim 20$ keV) prompt emission phase of GRB 100316D is reminiscent of GRB 060218 and it has been studied by Starling et al. (2011)

and Fan et al. (2011). Spectroscopic follow-up showed the emergence of clear SN features several days after the trigger. The associated SN, called SN 2010bh, exhibited spectral features indicating a hydrogen-stripped progenitor and evolved similarly to previous GRB-SNe (Chornock et al. 2010; Cano et al. 2011; Olivares E. et al. 2012; Bufano et al. 2012).

Here we present the results from a broad-band, late-time monitoring of the sub-energetic GRB 100316D at X-ray and radio wavelengths. Our observations constrain the explosion energy, its geometry, and the properties of its environment, previously shaped by the progenitor mass-loss. We find evidence for a quasi-spherical, central-engine-driven explosion with mildly relativistic ejecta. In contrast to ordinary GRBs, emission from the central engine of GRB 100316D dominates over the standard afterglow at late-times, allowing us to discuss its properties in the context of black-hole and magnetar progenitors.

Throughout this paper, we use the convention $F_\nu(\nu, t) \propto \nu^{-\beta}\, t^{-\alpha}$, where the spectral energy index is related to the spectral photon index by $\Gamma = 1 + \beta$. Uncertainties are quoted at a 68% confidence level unless otherwise noted. Standard cosmological parameters have been employed: $H_0 = 71$ km s^{-1} Mpc^{-1}, $\Omega_\Lambda = 0.73$, and $\Omega_M = 0.27$.

2. OBSERVATIONS

2.1. X-rays

The *Swift* X-Ray Telescope (XRT; Burrows et al. 2005) began observing GRB 100316D 127.5 s after the trigger, revealing a flat and smooth X-ray light-curve (Figure 1) reminiscent of the sub-luminous GRB 060218 (Campana et al. 2006). The early-time ($\Delta t < 0.1$ days) X-ray emission of GRB 100316D was extensively studied by Starling et al. (2011), who report the presence of a thermal blackbody component, later questioned by Fan et al. (2011). Our main focus is on the late-time ($\Delta t > 0.5$ days) X-rays.

We analyzed the XRT data using the latest HEAsoft release (v6.13), with standard filtering and screening criteria, and generated the 0.3–10 keV light curve following the procedure outlined in Margutti et al. (2013). The use of the latest XRT calibration files (v13) leads to a severe reduction of the statistical significance associated with the thermal blackbody component, with a chance probability of 10^{-3} (using v13) versus 10^{-10} (using v11), according to the *F*-test. In their re-analysis of the early X-ray data, Starling et al. 2012 found a similar trend (see their Table 2). Given the strong dependence of the statistical significance of the blackbody component on the instrumental calibration and the very limited impact[8] on the intrinsic neutral hydrogen column density estimate N_{H_z}, in the following we adopt $N_{H_z} = (0.68 \pm 0.02) \times 10^{22}$ cm^{-2}, as obtained from a simple power-law spectral fit to the data between 127 s and 737 s, where no spectral evolution is apparent. The best fitting photon index is $\Gamma_x = 1.42 \pm 0.02$ and the Galactic column density is $N_H = 7.1 \times 10^{20}$ cm^{-2} (Kalberla et al. 2005).

At late times, the X-ray emission from GRB 100316D significantly softens. A spectrum extracted in the time interval 0.4–2.1 days (rest-frame) is well fit by an absorbed power-law model with an exceptionally soft photon index $\Gamma_x = 3.49 \pm 0.26$. At this epoch, GRBs typically show $\Gamma_x \sim 2$ (Margutti et al. 2013). This uncommon spectral behavior was previously observed in GRB 060218 (Fan et al. 2006).

[8] From a black body plus power-law spectral fit, the best fitting intrinsic absorption is $N_{H_z} = (0.81 \pm 0.07) \times 10^{22}$ cm^{-2}. The black body only contributes ~1.5% to the total 0.3–10 keV fluence.

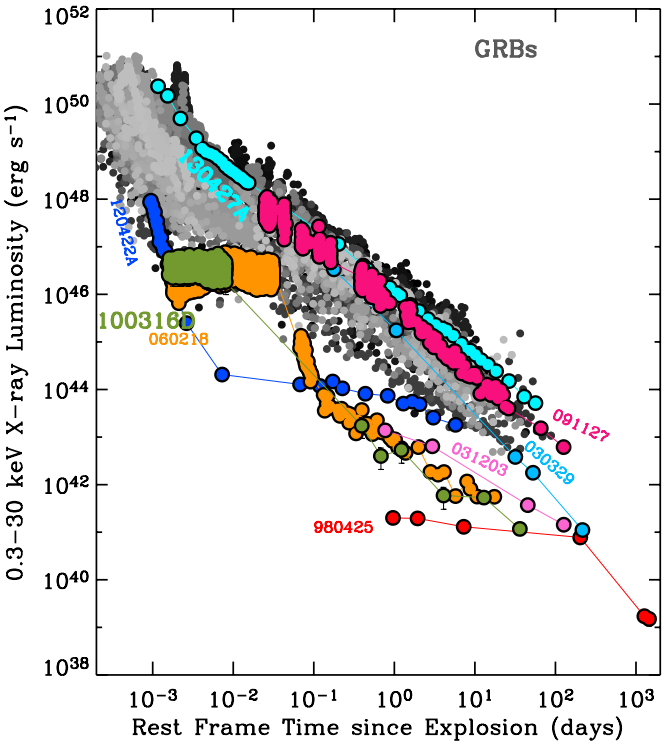

Figure 1. X-ray luminosity of GRB 100316D (including *Swift*-XRT and *Chandra*) compared to the sample of 165 long GRBs with redshift observed by *Swift*-XRT between 2004 and the end of 2010 in the common rest-frame energy band 0.3–30 keV from Margutti et al. (2013). To this sample we add GRB 980425 (Pian et al. 2000; Kouveliotou et al. 2004), GRB 031203 (Watson et al. 2004), GRB 030329 (Tiengo et al. 2004), GRB 120422A, and GRB 130427A. GRBs with spectroscopically associated SNe are in color and labeled. GRB 100316D is similar to GRB 060218 at both early and late times. Around $t \sim 40$ days, the X-ray luminosity of GRB 100316D approaches the level of GRB 980425, the least luminous X-ray afterglow ever detected.

(A color version of this figure is available in the online journal.)

Motivated by the long-lived and peculiar afterglow of previous nearby GRB-SNe, we initiated a deep X-ray follow up of GRB 100316D with the *Chandra X-Ray Observatory*. Observations were obtained on 2010 March 30.3 and April 23.8 UT ($\Delta t \approx 13.8$ and 38.3 days) for 14 and 30 ks, respectively (Program 11500488; PI: Soderberg). *Chandra* ACIS-S data were reduced with the `CIAO` software package (v4.3), using the calibration database CALDB v4.4.2, and applying standard ACIS data filtering. In both observations, we detected a source coincident with the *Swift*/XRT and radio positions (see Section 2.2) with a significance of $\sim 6\sigma$ according to `wavdetect`. Using a 1.″5 aperture, the source count rate in the 0.5–8 keV range is $(8.1 \pm 2.6) \times 10^{-4}$ ct s^{-1} and $(4.9 \pm 1.4) \times 10^{-4}$ ct s^{-1} for the first and second epoch, respectively. Assuming the spectral parameters from the XRT analysis, the count rates translate to an unabsorbed 0.3–10 keV flux of $(5.0 \pm 1.3) \times 10^{-14}$ erg cm^{-2} s^{-1} (first epoch) and $(2.7 \pm 0.7) \times 10^{-14}$ erg cm^{-2} s^{-1} (second epoch).

Figure 1 shows the complete X-ray data set, with observations from 100 s until 40 days since the explosion. Compared with a representative sample of GRBs in the common rest frame 0.3–30 keV band from Margutti et al. (2013), GRB 100316D is among the least luminous, both during the prompt and during the late-time afterglow phase. At ~40 days, GRB 980425 and GRB 100316D are the least luminous GRB explosions ever detected.

Table 1
ATCA Observations of GRB 100316D/SN 2010bh

Date (UT)	Time (Obs. Frame) (days)	$F_{\nu,5.4}$ (μJy)	$F_{\nu,9.0}$ (μJy)
2010 Mar 18.35	1.81	<78	<120
2010 Mar 27.10	10.57	<81	<135
2010 Apr 4.46	18.93	90 ± 20	<63
2010 Apr 15.40	29.87	128 ± 19	81 ± 26
2010 Apr 22.50	36.97	68 ± 21	<72
2010 May 25.40	69.87	50 ± 16	<60
2010 Sep 6.77	174.24	<42	<60

Note. Errors are 1σ and upper limits are 3σ.

2.2. Radio

We observed GRB 100316D with the Australia Telescope Compact Array (ATCA) from 2010 March 18.35 UT to September 6.77 UT ($\Delta t \approx 1.8$–174 days) using the Compact Array Broadband Backend (Wilson et al. 2011). All observations were carried out at 5 and 9 GHz, with a bandwidth of 2 GHz and are reported in Table 1. We used PKSB1934-638 for flux calibration, while phase referencing was performed using the calibrator PKSB0742-56 at the improved position reported by Petrov et al. (2011). We reduced the data using the MIRIAD package (Sault et al. 1995).

No radio source was detected in our first observation at $t \approx 1.8$ days, enabling a deep limit of $F_\nu \lesssim 78$ and $120\,\mu$Jy (3σ rms) at 5.4 and 9.0 GHz, respectively (Wieringa et al. 2010). A similarly deep observation at $t \approx 10.6$ days also revealed no counterpart at either frequency. However, on April 4.5 UT ($t \approx 19.0$ days), we clearly detected a 5.4 GHz source within the XRT error circle at 6.5σ significance. Fitting a point source model, we measured an integrated flux density of $F_\nu \approx 90 \pm 20\,\mu$Jy. A contemporaneous observation at 9 GHz constrained $F_\nu \lesssim 63\,\mu$Jy (3σ). From our observations on April 15.4, the radio source is located at position $\alpha(\mathrm{J2000}) = 07^{\mathrm{h}}10^{\mathrm{m}}30\overset{\mathrm{s}}{.}47$, $\delta(\mathrm{J2000}) = -56^{\circ}15'20\overset{''}{.}03$, with an uncertainty of $\pm 0\overset{''}{.}4$ in each coordinate. The radio afterglow of GRB 100316D was detected at 5.4 GHz until $t \approx 70$ days. Our monitoring reveals a temporal peak around 30 days at $\sim$5 GHz.

When compared to other GRB afterglows in Figure 2, GRB 100316D competes with the least luminous radio afterglows ever detected, with a luminosity between the sub-energetic GRBs 060218 and 980425. The timescale of the temporal peak is, however, much later than for GRB 060218.

3. PROPERTIES OF THE LATE-TIME X-RAY EMISSION

The late-time X-ray emission of GRB 100316D is characterized by a mild decay $\propto t^{-\alpha_x}$ with an index of $\alpha_x = 0.87 \pm 0.08$ (for $t > 0.3$ days, rest frame, see Figure 3), compared to the steeper decay $\alpha_x \sim 1.4$ typically observed in GRB afterglows at this epoch (Figure 4). The X-ray spectrum is unusually soft, with a power-law spectral energy index of $\beta_x = 2.49 \pm 0.26$. The low luminosity and exceptional spectral softness clearly distinguish GRBs 100316D and 060218 from all other GRBs and GRB-SNe of Figure 4. Independent of the X-rays being above or below the synchrotron cooling frequency ν_c, $\beta_x \sim 2.5$ implies a very steep distribution of shocked electrons $n_e(\gamma) \propto \gamma^{-p}$, with $p = 5$–6. In the standard external forward shock model, such a steep electron distribution would naturally produce a fast-decaying light curve with $\alpha_x > 3.3$, significantly steeper than the observed $\alpha_x \sim 0.9$ (Figure 5). The exceptionally soft spectrum and the

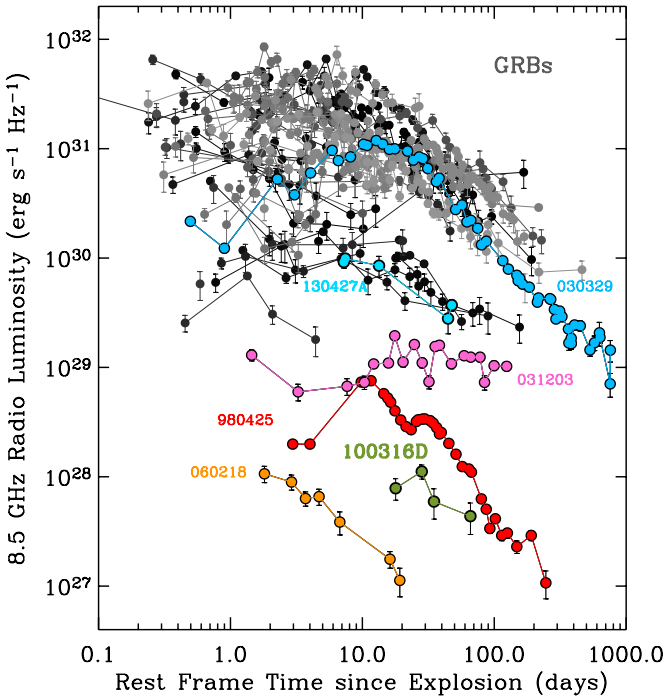

Figure 2. 8.5 GHz (rest-frame) radio afterglow of GRB 100316D compared to the radio-selected sample of 129 GRBs observed between 1997 and the end of 2011, for which a redshift measurement is available, presented in Chandra & Frail (2012). To this sample we add GRB 130427A, using radio observations by Laskar et al. (2013) and Perley et al. (2013). GRBs with spectroscopically associated SNe are in color and labeled. With a luminosity between GRB 060218 and GRB 980425 at $t \sim$ 10–70 days, GRB 100316D competes with the least luminous GRB radio afterglows ever detected.

(A color version of this figure is available in the online journal.)

milder than average temporal decay are therefore not consistent with the standard external forward shock origin.

The dynamics of the forward shock above would, however, be modified by continuous energy injection by the central engine into the shock. Following Zhang et al. (2006), we consider an injection luminosity term scaling as $L(t) = L_0(t/t_0)^{-q}$. The energy in the fireball scales as $E \propto t^{1-q}$. The mild temporal decay of GRB 100316D and its super soft X-ray spectrum would require an injection luminosity index $q < -0.3$, implying a rising injected luminosity with time (Zhang et al. 2006, their Table 2). GRB progenitor models either lead to a black hole torus system (e.g., Narayan et al. 1992; Woosley 1993; Paczynski 1998; Meszaros et al. 1999; Fryer et al. 1999) or to a highly magnetized, rapidly rotating pulsar (i.e., a magnetar, e.g., Usov 1992; Duncan & Thompson 1992). The initial spin-down luminosity from a millisecond pulsar requires $q = 0$, evolving to $q = 2$ at later times, when the electromagnetic dipolar radiation dominates (e.g., Dai & Lu 1998; Zhang & Mészáros 2001). The injection luminosity term of a black hole torus system is typically characterized by $q = 5/3$ (or $q = 4/3$) at late times (MacFadyen et al. 2001; Janiuk et al. 2004 and references therein), and hence has no impact on the dynamics of an adiabatic fireball (for which $q < 1$ is required; Zhang & Mészáros 2001). A study of X-ray flares in GRBs points to an even steeper index $q \sim 2.7$ (Margutti et al. 2011) at earlier times. For both a magnetar and a black hole system, the injected luminosity index is therefore $q \geqslant 0$, not consistent with $q < -0.3$ required to explain the properties of the late-time X-ray emission of GRB 100316D. We conclude that the late-time X-rays are unlikely to originate from the emission

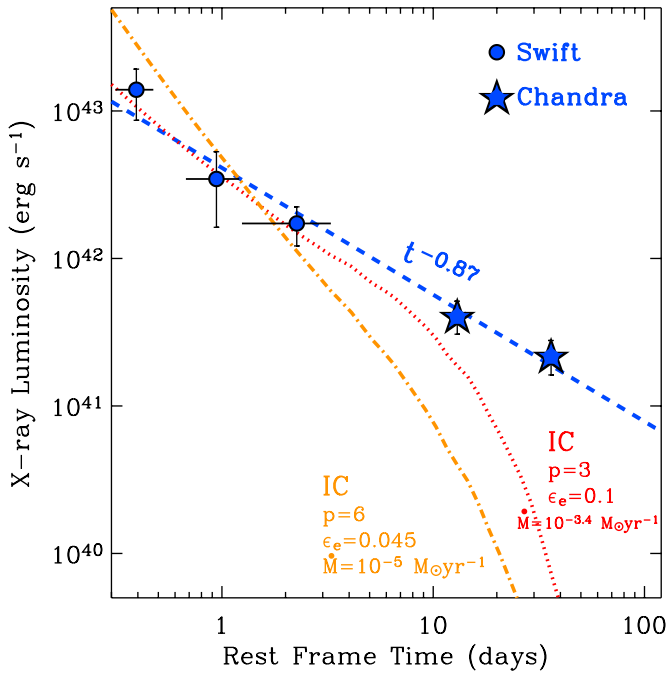

Figure 3. Late-time evolution of the X-ray afterglow of GRB 100316D as revealed by *Swift* and *Chandra* observations in the 0.3–10 keV (observer frame) energy band. The best-fitting power-law decay is $\propto t^{-0.87\pm0.08}$ (dashed blue line). The expected contribution from Inverse Compton (IC) emission originating from up-scattered SN photospheric photons by a population of electrons with $p = 3$ (dotted red line) and $p = 6$ (dot-dashed orange line) that best fits the observations is also shown. For $t > 10$ days, IC radiation substantially under predicts the observed luminosity and cannot explain the persistent late-time X-ray emission.

(A color version of this figure is available in the online journal.)

from the explosion shock decelerating into the environment. This conclusion is independently supported by the analysis of the contemporaneous radio emission in Section 4. Alternative scenarios are explored in Section 6.

4. LATE-TIME RADIO-TO-X-RAYS ENERGY DISTRIBUTION

We study the radio-to-X-rays spectral energy distribution (SED) at six different epochs corresponding to the times of the radio observations in Table 1. At these times, the optical wavelengths are dominated by the SN photospheric emission and are therefore not included here. In the standard afterglow scenario, radio and X-ray photons originate from the same population of electrons accelerated to relativistic speed by the explosion shock and are expected to lie on the same synchrotron spectrum (e.g., Granot & Sari 2002, their Figure 1). We test this prediction below.

An SED extracted at $t = 1.7$ days (rest frame) constrains the radio-to-X-ray spectral index to an unusually flat value, $\beta_{RX} < 0.6$. A similar value was observed only in the case of GRB 060218, for which $\beta_{RX} = 0.5$ a few days after the explosion (Soderberg et al. 2006a). At this time, the X-rays show an uncommon, exceptionally steep spectrum, with $\beta_X \sim 2.5$ (Section 3 and Figure 4).

Further radio observations at $t = 17.9$ days indicate a decreasing radio flux density with frequency, $F_R \propto \nu^{-\beta_R}$ with $\beta_R > 0.78$, implying that by this time, the spectral peak frequency has crossed the radio band and $\nu_{\rm sa} \lesssim 9$ GHz, (where $\nu_{\rm sa}$ is the synchrotron self-absorption frequency). We use the constraint $\beta_R > 0.78$ to compute an upper limit to the contemporaneous X-ray radiation originating from synchrotron emission. Figure 6 shows the results at $t = 34.9$ days (rest-frame). The observed X-ray flux is significantly brighter than the extrapolation of the synchrotron model even in the most optimistic case of a simple power-law spectral distribution with $\beta = 0.78$. We conclude that even if we ignore the exceptionally soft X-ray spectrum, the synchrotron model is unable to explain the late-time X-ray emission in GRB 100316D, which should be interpreted as a different component (Section 6). For $t > 1$ day, X-ray and radio photons cannot be connected with the emission from a single shock wave. It is remarkable that the observed late-time X-ray and radio emission of GRB 060218 shares these same properties and points to the same conclusion (Soderberg et al. 2006a; Fan et al. 2006; see also Waxman et al. 2007).

5. RADIO CALORIMETRY AND JET OPENING ANGLE

Using the radio afterglow of GRB 100316D, we constrain its kinetic energy, jet opening angle, and density of the environment. Observations at $t_1 \sim 18$ days (rest-frame) indicate that the spectral peak frequency is just below the radio band, $\nu_{\rm sa}(t_1) \lesssim 9$ GHz, while the peak of the light-curve around $t_2 \sim 30$ days suggests that $\nu_{\rm sa}(t_2) \sim 5$ GHz, with $F_{\nu_{sa}} \sim 130\,\mu$Jy. Applying the standard formulation of GRB afterglows powered by synchrotron emission (Granot & Sari 2002, their Table 2) and assuming a wind-like $n \propto r^{-2}$ environment as appropriate for massive stars at the end of their evolution, we constrain the fireball kinetic energy, E_k, and the progenitor mass-loss rate, $A_\star$ (defined following Chevalier & Li 2000). For an electron power-law index $p = 2.1$–2.3 and microphysical parameters $\epsilon_e = 0.01$–0.1, $\epsilon_B = 0.01$, the fireball kinetic energy is $E_k = (0.3$–$4) \times 10^{49}$ erg coupled to mildly relativistic ejecta with $\Gamma \sim 1.5$–2 (at one day rest-frame).[9] The mass-loss rate is $A_\star = 0.4$–1 corresponding to $\dot{M} = (0.4$–$1) \times 10^{-5}\,M_\odot\,{\rm yr}^{-1}$ for wind velocity $v_w = 1000\,{\rm km\,s}^{-1}$. Compared with its cosmic twin GRB 060218, GRB 100316D is $\sim$10 times more energetic, but exploded in a much denser environment.[10] The higher environment density of GRB 100316D explains why the blast wave associated with the less energetic GRB 060218 propagates with comparable but higher velocity: Soderberg et al. (2006a) infer $\Gamma \sim 2.3$ at $t \sim 5$ days. The progenitor of GRB 100316D suffered from more consistent mass-loss before exploding, causing the fireball to decelerate on shorter timescales compared to shocks propagating in less dense environments like GRB 060218, for which $\dot{M} \sim \times 10^{-7}\,M_\odot\,{\rm yr}^{-1}$ (Soderberg et al. 2006a).

The late-time temporal decay of the radio light-curve $\propto t^{-\alpha_r}$ with $\alpha_r < 1$ is much shallower than the $t^{-2.2}$ behavior expected after a jet break (Sari et al. 1999) and suggests that the fastest ejecta responsible for the radio emission is not strongly collimated. Our radio monitoring constrains the jet break time $t_j > 66$ days (rest-frame) which formally translates into a jet opening angle $\theta_j > 80^\circ$, for the kinetic energy and environment density determined above (see Chevalier & Li 2000, their Equation (31)). As for GRB 060218 (for which $\theta_j > 80^\circ$, Soderberg et al. 2006a), the radio observations argue for a mildly relativistic explosion with quasi-spherical ejecta.

[9] For an interstellar medium (ISM) environment, we find $E_k \approx 0.5 \times 10^{49}$ erg, density $n_0 \gtrsim 50\,{\rm cm}^{-3}$.

[10] This suggests that the high $NH_z \sim 7 \times 10^{21}$ cm^{-2} of Section 2.1is local to the explosion, as opposed to arising from material that happens to be along our line of sight. For comparison, this value is a factor $\sim$2 higher than the NH_z inferred for GRB 060218 (Soderberg et al. 2006a).

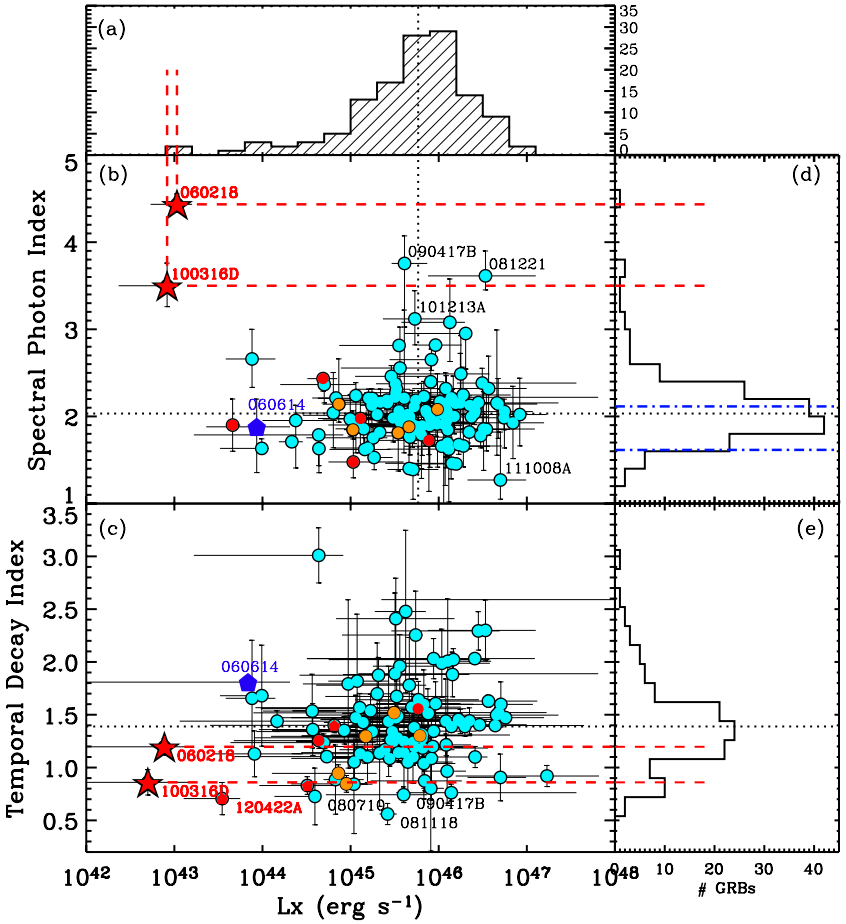

Figure 4. Temporal and spectral properties of the late-time X-ray emission for a sample of 112 GRBs detected by *Swift* between 2004 November and 2013 July, with known redshift. GRBs with spectroscopically confirmed SNe are in red. GRBs with photometrically associated SNe are in orange. The blue diamond identifies the SN-less GRB 060614 (Della Valle et al. 2006; Fynbo et al. 2006). The dotted lines mark the median values of the distributions. Panel (b): X-ray spectral photon index Γ_x computed in the rest-frame time interval 0.5–2 days as a function of the X-ray luminosity in that time interval (median value). Panel (c): temporal decay index α_x as obtained from a local fit of the X-ray light-curves between 0.5 and 10 days, rest-frame. Panels (a)–(e): projected distributions. The dot-dashed lines in panel (d) mark the predicted Γ_x that follows from the general expectation of an electron power-law distribution $n_e(\gamma) \propto \gamma^{-p}$ with $p \sim 2.23$ in relativistic shocks with Fermi acceleration (Kirk et al. 2000; Keshet & Waxman 2005), depending on whether the X-rays lie on the $F_x \propto \nu^{-p/2}$ (upper line) or the $F_x \propto \nu^{-(p-1)/2}$ (lower line) spectral segment. GRBs 100316D and 060218 are clearly distinguished from all the other GRBs because of their extreme spectral softness and low luminosity. The decay of their X-ray light-curve is also shallower than average.

(A color version of this figure is available in the online journal.)

These properties place the sub-energetic GRB 100316D between the highly relativistic, collimated GRB explosions and the spherical, ordinary Type Ib/c SNe as we show in Figure 7. Its kinetic energy profile $E_k \propto (\Gamma\beta)^{-2.6}$ is significantly flatter[11] than that expected from a pure hydrodynamic collapse (where $E_k \propto (\Gamma\beta)^{-5.2}$, Tan et al. 2001), and argues for the presence of a central engine able to accelerate a non-negligible fraction of the ejecta to mildly relativistic speeds. A flatter $E_k(\Gamma\beta)$ profile is expected for jet-driven stellar explosions (Lazzati et al. 2012), with the least steep $E_k(\Gamma\beta)$ profiles associated with powerful jets able to break out through the stellar surface while the engine is still active. Highly relativistic GRBs belong to this category of explosions and show $E_k \propto (\Gamma\beta)^{-\delta}$ with $\delta < 1$ (Figure 7). GRB 100316D instead seems to be associated with the class of jet-driven explosions where the jet head is only barely able to reach the surface (or even breaks out after the end of the central engine activity), resulting in an $E_k(\Gamma\beta)$ profile intermediate between a pure hydrodynamic collapse (where no jet is formed at any stage of the collapse) and that of fully developed, jet-powered explosions.

[11] The dense environment around GRB 100316D significantly decelerated the fastest ejecta by one day after the explosion, the time at which we compute $\Gamma\beta$ in Figure 7. The "intrinsic" $E_k(\Gamma\beta)$ profile of the explosion is therefore flatter than what is shown.

6. NATURE OF THE LATE-TIME X-RAY EMISSION

GRB 100316D is characterized by an unusually flat radio to X-ray spectral index, an exceptionally soft late-time X-ray emission, and a flatter than average X-ray temporal decay (Section 3). These properties led us to identify the presence of an X-ray excess of emission with respect to the standard afterglow model powered by synchrotron radiation (Section 4). Here we discuss the physical origin of the excess of emission and conclude that this excess is connected to the explosion central engine.

6.1. Inverse Compton Emission

Inverse Compton (IC) emission originating from the up-scattering of optical photons from the SN photosphere by a population of electrons accelerated to relativistic speeds by the shock wave potentially contributes to the observed X-ray emission. The IC X-ray emission is negligible for cosmological GRBs, but might be relevant for nearby bursts. In ordinary

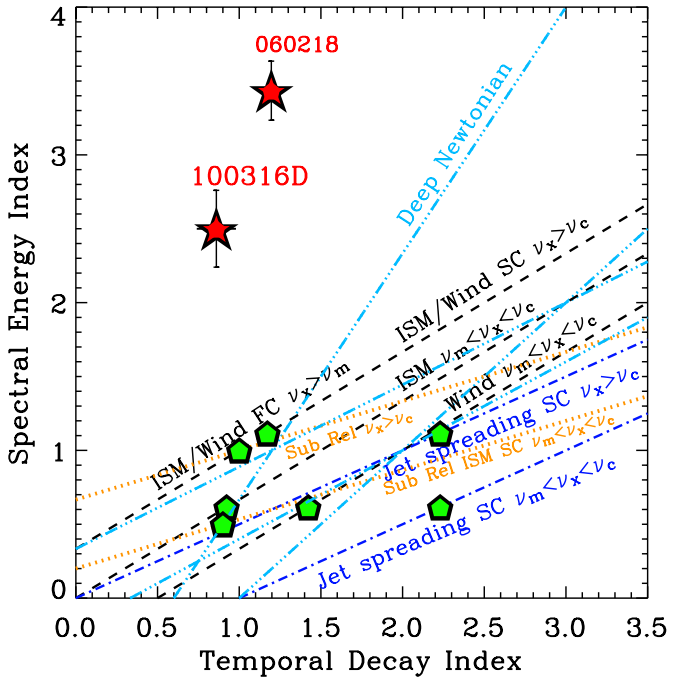

Figure 5. Late-time (0.5–10 days) X-ray spectral energy index β_x and temporal decay slope α_x of GRB 100316D compared to the expectations from synchrotron radiation from a relativistic shock expanding into an ISM or wind-like medium (black dashed lines, Zhang & Mészáros 2004; Zhang et al. 2006), in the fast-cooling (FC) or slow-cooling (SC) regimes. ν_c refers to the synchrotron cooling frequency, while ν_m is the characteristic synchrotron frequency. Blue dot-dashed lines: uniform jet spreading with time (relativistic). We only plot closure relations for $p > 2$ as indicated by our analysis in Section 3. Orange dotted lines: closure relations for a sub-relativistic shock (Frail et al. 2000). Light-blue, triple dot-dashed lines: expected β_x–α_x relations for a shock in the deep Newtonian phase (Sironi et al. 2013). The green diamonds mark the position of a blast wave with a power-law population of radiating electrons with $p = 2.23$ (as expected for relativistic shocks; Kirk et al. 2000; Keshet & Waxman 2005) or $p = 2$ (general expectation for non-relativistic shocks, e.g., Blandford & Eichler 1987). GRBs 100316D and 060218 are clearly *not* consistent with these predictions.

(A color version of this figure is available in the online journal.)

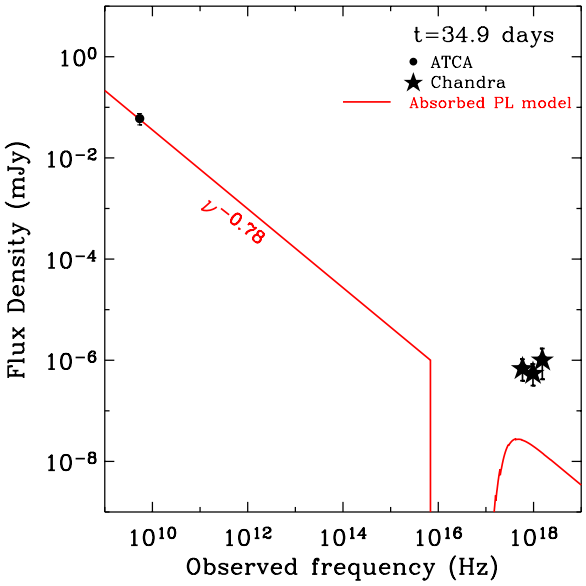

Figure 6. Radio-to-X-ray SED at $t = 34.9$ days (rest frame) revealing the presence of an excess of X-ray radiation with respect to the expected synchrotron emission (red solid line). Here we show the most optimistic spectral model with $F_\nu \propto \nu^{-0.78}$. Radio observations at $t = 17.9$ days (rest frame) indicate $\beta_R > 0.78$. A spectral break between radio and X-rays would lead to an even more pronounced X-ray excess, leading us to conclude that the synchrotron forward shock model is unable to explain the bright late-time X-ray emission.

(A color version of this figure is available in the online journal.)

hydrogen-stripped SNe exploding in low-density environments, IC is the main X-ray emission mechanism during the first ∼40 days after the explosion (Björnsson & Fransson 2004; Chevalier & Fransson 2006). We estimate the expected IC contribution to the X-ray afterglow of GRB 100316D by employing the formalism by Margutti et al. (2012) modified to account for a SN ejecta outer density structure scaling as $\rho_{\rm SN} \propto R^{-n}$ with $n \sim 10$, as appropriate for Type Ib/c SNe (Matzner & McKee 1999). The IC X-ray luminosity depends on the structure and density of the environment swept up by the blast wave $\rho_{\rm CSM}(R)$; the details of the electron distribution $n_e(\gamma) = n_0\gamma^{-p}$ responsible for the up-scattering; the fraction of shock energy in relativistic electrons ϵ_e; the explosion parameters (ejecta mass $M_{\rm ej}$ and kinetic energy $E_{\rm k}$), and the SN bolometric luminosity ($L_{\rm IC} \propto L_{\rm bol}$).

The bolometric luminosity of SN 2010bh has been computed by Bufano et al. (2012). Their modeling of the bolometric light curve points to an energetic SN explosion with $E_{\rm k} \sim 10^{52}$ erg and $M_{\rm ej} \sim 3\,M_\odot$ (see also Cano et al. 2011, Olivares E. et al. 2012, and Cano 2013, who obtained consistent results considering the different extinction corrections adopted by the authors). Using these values and a wind-like circumstellar medium (CSM) ($\rho_{\rm CSM} \propto R^{-2}$, as expected from a star which has been losing material at constant rate $\dot{M}$), we show in Figure 3 the IC models that best fit our observations. We show the results for both a population of radiating electrons with $p = 3$, as typically indicated by radio observations of type Ib/c SNe (e.g., Chevalier & Fransson 2006), and for electrons with a much steeper distribution with $p = 6$, as suggested by the exceptionally soft late-time X-ray spectrum of GRB 100316D. The mass-loss rate, $\dot{M}$, is reported in Figure 3 for a wind velocity $v_w = 1000\,{\rm km\,s^{-1}}$, typical of Wolf–Rayet stars.

Irrespective of the assumed electron density distribution, the IC X-ray luminosity declines steeply after SN 2010bh reaches maximum light around $t \sim 10$ days (see Olivares E. et al. 2012, their Figure 7) due to the substantial decrease of optical seed photons from the SN photosphere. As a consequence, the IC mechanism severely underpredicts the observed luminosity at late times (Figure 3), failing to explain the persistent late-time X-ray emission in GRB 100316D. The fully relativistic treatment of the IC emission by Waxman et al. (2007) leads to the same conclusion.

6.2. Shock Break Out

GRB 060218 is the only other known explosion that shares the same unusual properties of the late time X-ray and radio emission with GRB 100316D (Figure 4), including evidence for an excess of soft X-ray radiation (Soderberg et al. 2006a; Fan et al. 2006). Both explosions are also characterized by a peculiar γ-ray prompt emission phase consisting of a smooth, long ($\Delta t > 1300$ s), and soft (time averaged spectral peak energy $E_{\rm pk} < 20$ keV) pulse of emission releasing a modest amount of energy $E_{\rm iso} \sim 5 \times 10^{49}$ erg (Kaneko et al. 2007; Starling et al. 2011), setting these two bursts apart from all the other GRBs. The properties of these two bursts also sets them apart from the handful of known sub-energetic GRBs as well. It is thus reasonable to believe that the physical origin of the unusual early-time and late-time properties is in some way related.

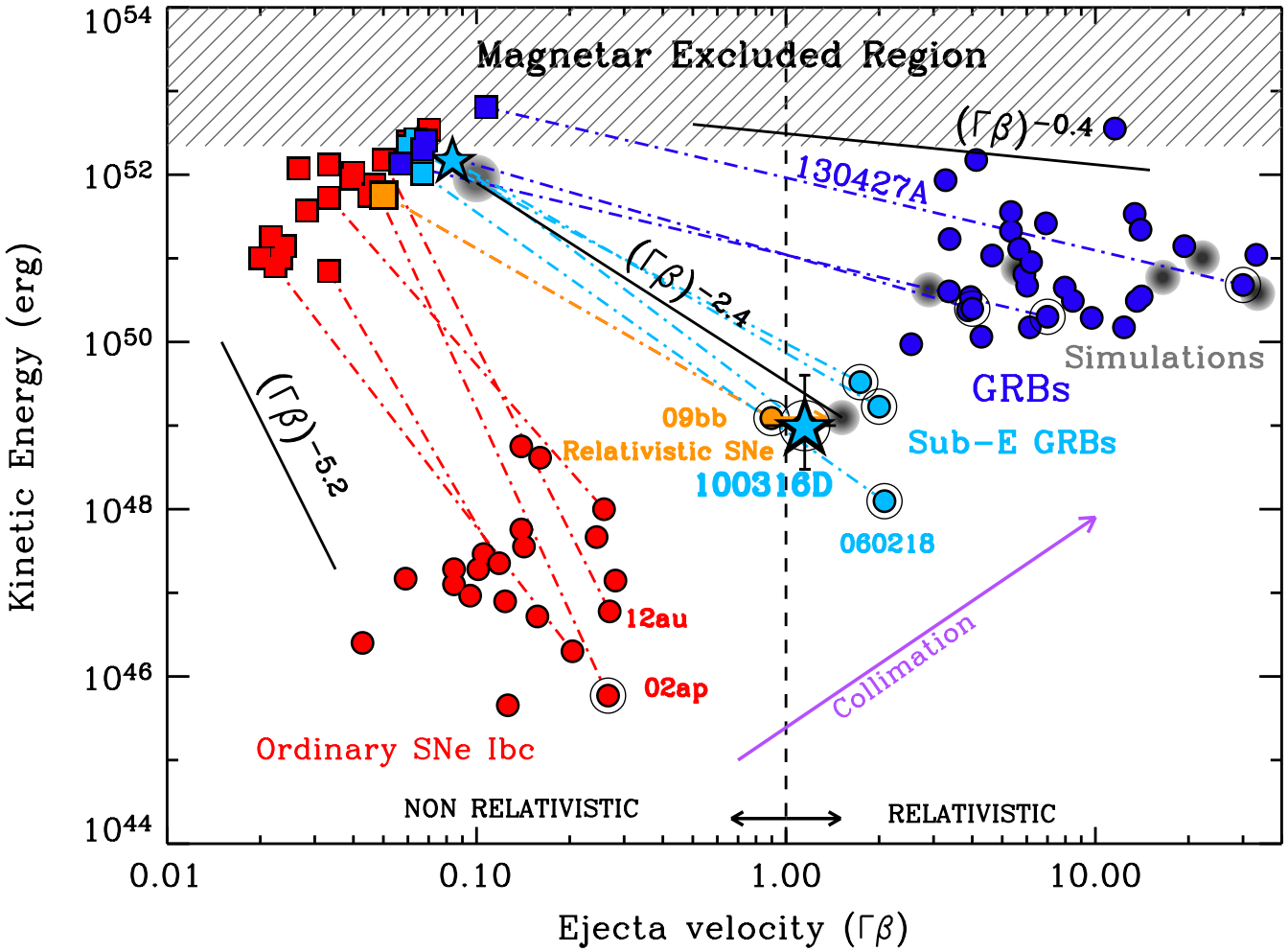

Figure 7. Kinetic energy–velocity profile of the ejecta of ordinary SNe Ib/c (red), relativistic SNe (orange), sub-energetic GRBs (light blue), and GRBs (blue). Squares: E_k in slow moving material estimated from the modeling of the SN optical emission. The circles mark the E_k in the fastest ejecta as measured from radio observations of SNe and broad-band afterglow modeling of GRBs, for which we report the beaming corrected values. For GRBs, $\Gamma\beta$ of the fast component is estimated at one day rest-frame and includes deceleration of the blast wave into the environment. The open black circles identify explosions with broad lines in their optical spectra. Gray points: results obtained from simulations of jet-driven explosions with energy $E = 2 \times 10^{52}$ erg and different duration of the central engine (Lazzati et al. 2012). The dashed-dotted lines connect measurements of the same explosion. Ordinary SNe are characterized by very steep profiles where a negligible fraction of energy is coupled to the fastest moving material, in general agreement with the expectations from pure hydrodynamic collapse $E_k \propto (\Gamma\beta)^{-5.2}$, where no central engine is involved (Tan et al. 2001). GRBs distribute their energy budget differently, with comparable energy in their relativistic (or mildly relativistic) and slow ejecta. The result is a much flatter E_k profile, typical of jet-driven explosions with long-lasting central engines ($E_k \propto (\Gamma\beta)^{-0.4}$ for an explosion energy of 2×10^{52} erg and engine duration of 7 s; Lazzati et al. 2012). Relativistic SNe and sub-energetic GRBs are intermediate ($E_k \propto (\Gamma\beta)^{-2.4}$), and fall into the parameter space occupied by weak jet-driven explosions where the jet barely pierces through the stellar surface (References: ordinary Type Ib/c SNe: Berger et al. 2003a; Soderberg et al. 2006a; Soderberg et al. 2008; Soderberg et al. 2010b; Soderberg et al. 2010a; Sanders et al. 2012; Cano 2013; Milisavljevic et al. 2013; Mazzali et al. 2013; Kamble et al. 2013. Sub-energetic GRBs: Berger et al. 2003b; Soderberg et al. 2006b and references therein; Cano 2013. Relativistic SN 2009bb: Soderberg et al. 2010b; Cano 2013. GRBs: Berger et al. 2003a; Frail et al. 2006; Chandra et al. 2008; Cenko et al. 2010; Cenko et al. 2011; Troja et al. 2012; Cano 2013; Xu et al. 2013; Laskar et al. 2013; Perley et al. 2013; Guidorzi et al. 2013).

(A color version of this figure is available in the online journal.)

The prompt emission of GRBs 060218 and 100316D have been explained by Nakar & Sari (2012)[12] as radiation from a relativistic shock breaking out at a large radius $R_{\rm bo} \sim 5 \times 10^{13}$ cm (for GRB 060218) and $R_{\rm bo} > 6 \times 10^{13}$ cm (for GRB 100316D, for which only a lower limit can be placed on the γ-ray energy $E_{\rm iso} > 6 \times 10^{49}$ erg due to an orbital data gap; Starling et al. 2011). By ~40 days after the explosion, the typical temperature of the shock break out radiation $T_{\rm bo}$ is, however, significantly below the X-ray band ($T_{\rm bo} \ll 0.1$ keV using the formalism by Nakar & Sari 2010, 2012), leading us to conclude that the contribution of residual radiation from the shock break out to the late-time X-rays is negligible.

[12] See also Waxman et al. (2007) and Wang et al. (2007) for GRB 060218.

6.3. Long-lived Central Engine

The $E_k(\Gamma\beta)$ profile of Section 5 (Figure 7) argues for the presence of a central engine and identifies GRB 100316D as one of the weakest central-engine-driven explosions detected so far. Here we consider the possibility of radiation originating from the explosion remnant, in the form of a long-lived central engine. The same possibility was considered by Fan et al. (2006) for GRB 060218. The collapse of massive stars typically leads to a black hole plus long-lived debris torus system (Narayan et al. 1992; Woosley 1993; Paczynski 1998; Meszaros et al. 1999; Fryer et al. 1999) or to a fast-rotating, highly magnetized pulsar (i.e., a magnetar, e.g., Usov 1992; Duncan & Thompson 1992).

Accretion onto a black hole is a well known source of high-energy radiation. From the observed $L_x \sim 3 \times 10^{41}$ erg s^{-1} at ∼30 days after the explosion, we estimate an accretion rate of $\dot{M}_{\rm acc} \sim 10^{-10}$–$10^{-8}\, M_\odot\, {\rm s}^{-1}$, assuming an accretion efficiency $\eta_{\rm acc} = 0.001$–0.01 (e.g., MacFadyen et al. 2001) and an X-ray to bolometric flux correction $\eta_x = 0.01$–0.1 (Fan et al. 2006). The inferred range of $\dot{M}_{\rm acc}$ is consistent with the extrapolation of the expected accretion rates from fall back calculated by MacFadyen et al. (2001) in the context of the collapsar model. This result would point to similar late-time accretion rates between bright bursts (for which the model by MacFadyen et al. 2001 was originally developed) and sub-energetic GRBs. The observed temporal decay $L_x \propto t^{-0.87}$ is, however, significantly shallower than what expected in the context of fall-back accretion models that predict $L \propto t^{-5/3}$ (e.g., Chevalier 1989). While the mild L_x decay does not rule out accretion as the source of the late-time X-ray excess of radiation, it does require substantial departure from the simple fall-back picture.

Alternatively, GRB 100316D could have signaled the birth of a magnetar. With $E_k \sim 10^{52}$ erg coupled to the non-relativistic ejecta (e.g., Bufano et al. 2012), GRB 100316D approaches the limit of the magnetar models (Figure 7).[13] For a maximally spinning, $1.4\, M_\odot$ proto-neutron star, the total energy release cannot exceed its rotation energy budget $E_{\rm tot} \sim 2.2 \times 10^{52}$ erg (e.g., Thompson et al. 2004). In order to power a $\sim 10^{52}$ erg explosion, the highly magnetized ($B \sim 10^{15}$ G) compact object is required to be born rapidly rotating (initial spin period $P \sim 1$ ms), suggesting that GRB 100316D is associated with the fastest and most extreme proto-magnetars. While a significant fraction of rotation energy might be extracted in a few seconds (e.g., Metzger et al. 2007), the spin-down luminosity from the newly born magnetar is a source of long-lasting emission decaying as $L_p \propto t^{-l}$, where $l = 2$ corresponds to the magnetic dipole spin down. As in the case of GRB 060218 (Soderberg et al. 2006a), the shallow L_x temporal decay argues for a spin-down braking index $n \approx 2$ (where $\dot{\nu} = -K\nu^n$ is the braking law and $n = 3$ is for the standard magnetic dipole radiation with constant magnetic field. ν is the pulsar spin frequency). Interestingly, a braking index $n < 3$ has been observed in very young pulsars (e.g., Livingstone et al. 2007). The very soft X-ray spectrum could be either intrinsic or the result of the interaction of the central engine radiation with material ejected by the progenitor (e.g., via multiple inelastic electron scatterings that suppress high energy radiation).

7. CONCLUSIONS

Broad-band late-time monitoring of the sub-energetic GRB 100316D associated with SN 2010bh at radio and X-ray wavelengths allowed us to constrain the properties of the explosion and its environment. The explosion is energetically dominated by the non-relativistic material which carries $E_k \sim 10^{52}$ erg. A modest $E_k \sim 10^{49}$ erg is coupled to quasi-spherical, mildly relativistic ($\Gamma = 1.5$–2) ejecta expanding into a medium previously shaped by the progenitor mass-loss. We infer a progenitor mass-loss rate of $\dot{M} \sim 10^{-5}\, M_\odot\, {\rm yr}^{-1}$, for an assumed wind density profile and wind velocity $v_w = 1000\, {\rm km\, s}^{-1}$ and microphysical parameters $\epsilon_e = 0.01$–0.1 and $\epsilon_B = 0.01$.

These properties are intermediate between the highly relativistic, collimated GRBs and the spherical, ordinary hydrogen-stripped SNe. Like GRBs, but different than ordinary Type Ib/c SNe, the kinetic energy profile of GRB 100316D argues for the presence of a central engine that drives the explosion. However, unlike GRBs, our broad-band spectral modeling clearly identifies the presence of an excess of soft X-ray radiation with respect to the synchrotron afterglow model at late times. This result leads us to conclude that the late-time ($t > 10$ days), non-thermal radio and X-ray emission do not originate from the same population of electrons and are likely attributable to two different components.

We connect the excess of soft X-ray radiation to long-lasting activity of the explosion central engine, either in the form of a black hole plus torus system, or a magnetar. The very high kinetic energy ($E_k \sim 10^{52}$ erg) carried by the non-relativistic ejecta of GRB 100316D implies that only the most rapidly rotating magnetars with spin period $P \sim 1$ ms can power the explosion. Accretion onto a compact object cannot be excluded, but requires some significant departure from the standard fall-back scenario.

GRB 060218 is the only other explosion to date where a similar super-soft X-ray excess has been identified at late times (Soderberg et al. 2006a; Fan et al. 2006; Waxman et al. 2007). However, given the intrinsic faintness of the central engine component, it is possible that a similar emission is ubiquitous in long GRBs, but easily overshone by the external shock afterglow associated with the highly relativistic jet.

Finally, GRB 100316D and its cosmic twin, GRB 060218, define a class of sub-energetic explosions that are clearly distinguished from ordinary GRBs and other sub-energetic GRBs (e.g., 120422A; B. A. Zauderer et al., in preparation) by (1) a very long and smooth γ-ray prompt emission phase ($\Delta t > 1000$ s) with spectral peak energy $E_{\rm pk} \sim 10$ keV, (2) shallower than average late-time decay of the X-ray light-curve, (3) exceptionally soft late-time X-ray spectrum, and (4) evidence for an excess of soft X-ray emission with respect to the external shock afterglow at late times. These two GRBs have also been claimed to show evidence for a thermal component in their early time X-ray afterglow (Campana et al. 2006; Starling et al. 2011). Our re-analysis, however, points to a substantially reduced statistical significance of the black-body component in the early time spectra of GRB 100316D.

Further progress in our understanding of central-engine-driven explosions strongly relies on the ability to constrain their energetics, collimation and environment properties. This is a task that can only be accomplished with coordinated efforts at radio and X-ray wavelengths at late times when the central engine reveals itself in the X-rays.

R.M. is indebted to Cristiano Guidorzi for many interesting discussions. R.M. and B.J.M. thank Dominic Ryan for useful conversations. R.M. thanks the KITP in Santa Barbara for support, hospitality, and the stimulating environment that partially inspired this work. R.B.D. was supported by an ERC advanced grant (GRB) and by the I-CORE Program of the PBC and the ISF (grant 1829/12). L.S. is supported by NASA through Einstein Postdoctoral Fellowship grant number PF1-120090 awarded by the *Chandra X-Ray Center*, which is operated by the Smithsonian Astrophysical Observatory for NASA under contract NAS8-03060. B.J.M. is supported by an NSF Astronomy and Astrophysics Post-doctoral Fellowship under award AST1102796. E.P. acknowledges support from INAF PRIN 2011. R.A.C. acknowledges support from NASA grant NNX12AF90G. Support for this work was provided by the

[13] For comparison, as much as $\sim 10^{54}$ erg can be extracted from the black hole plus long-lived debris torus system (e.g., Meszaros et al. 1999).

David and Lucile Packard Foundation Fellowship for Science and Engineering awarded to A.M.S. The Australia Telescope Compact Array is part of the Australia Telescope National Facility which is funded by the Commonwealth of Australia for operation as a National Facility managed by CSIRO.

REFERENCES

Berger, E., Kulkarni, S. R., Frail, D. A., & Soderberg, A. M. 2003a, ApJ, 599, 408
Berger, E., Kulkarni, S. R., Pooley, G., et al. 2003b, Natur, 426, 154
Björnsson, C.-I., & Fransson, C. 2004, ApJ, 605, 823
Blandford, R., & Eichler, D. 1987, PhR, 154, 1
Bromberg, O., Nakar, E., & Piran, T. 2011, ApJL, 739, L55
Bufano, F., Pian, E., Sollerman, J., et al. 2012, ApJ, 753, 67
Burrows, D. N., Hill, J. E., Nousek, J. A., et al. 2005, SSRv, 120, 165
Campana, S., Mangano, V., Blustin, A. J., et al. 2006, Natur, 442, 1008
Cano, Z. 2013, MNRAS, 434, 1098
Cano, Z., Bersier, D., Guidorzi, C., et al. 2011, ApJ, 740, 41
Cenko, S. B., Frail, D. A., Harrison, F. A., et al. 2010, ApJ, 711, 641
Cenko, S. B., Frail, D. A., Harrison, F. A., et al. 2011, ApJ, 732, 29
Chandra, P., Cenko, S. B., Frail, D. A., et al. 2008, ApJ, 683, 924
Chandra, P., & Frail, D. A. 2012, ApJ, 746, 156
Chevalier, R. A. 1989, ApJ, 346, 847
Chevalier, R. A., & Fransson, C. 2006, ApJ, 651, 381
Chevalier, R. A., & Li, Z.-Y. 2000, ApJ, 536, 195
Chornock, R., Berger, E., Levesque, E. M., et al. 2010, arXiv:1004.2262
Cobb, B. E., Bailyn, C. D., van Dokkum, P. G., & Natarajan, P. 2006, ApJL, 645, L113
Dai, Z. G., & Lu, T. 1998, A&A, 333, L87
Della Valle, M., Chincarini, G., Panagia, N., et al. 2006, Natur, 444, 1050
Duncan, R. C., & Thompson, C. 1992, ApJL, 392, L9
Fan, Y.-Z., Piran, T., & Xu, D. 2006, JCAP, 09, 013
Fan, Y.-Z., Zhang, B.-B., Xu, D., Liang, E.-W., & Zhang, B. 2011, ApJ, 726, 32
Frail, D. A., Cameron, P. B., Kasliwal, M., et al. 2006, ApJL, 646, L99
Frail, D. A., Kulkarni, S. R., Sari, R., et al. 2001, ApJL, 562, L55
Frail, D. A., Waxman, E., & Kulkarni, S. R. 2000, ApJ, 537, 191
Fryer, C. L., Woosley, S. E., & Hartmann, D. H. 1999, ApJ, 526, 152
Fynbo, J. P. U., Watson, D., Thöne, C. C., et al. 2006, Natur, 444, 1047
Galama, T. J., Vreeswijk, P. M., van Paradijs, J., et al. 1998, Natur, 395, 670
Gehrels, N., Chincarini, G., Giommi, P., et al. 2004, ApJ, 611, 1005
Granot, J., & Sari, R. 2002, ApJ, 568, 820
Guetta, D., & Della Valle, M. 2007, ApJL, 657, L73
Guidorzi, C., Zauderer, B. A., Kobayashi, S., et al. 2013, ApJ, submitted
Hjorth, J., & Bloom, J. S. 2012, in Cambridge Astrophys. Ser. 51, Gamma-Ray Bursts, ed. C. Kouveliotou, R. A. M. J. Wijers, & S. Woosley (Cambridge: Cambridge Univ. Press), 169
Janiuk, A., Perna, R., Di Matteo, T., & Czerny, B. 2004, MNRAS, 355, 950
Kalberla, P. M. W., Burton, W. B., Hartmann, D., et al. 2005, A&A, 440, 775
Kamble, A., Soderberg, A., Chomiuk, L., et al. 2013, ApJ, submitted (arXiv:1309.3573)
Kaneko, Y., Ramirez-Ruiz, E., Granot, J., et al. 2007, ApJ, 654, 385
Keshet, U., & Waxman, E. 2005, PhRvL, 94, 1102
Kirk, J. G., Guthmann, A. W., Gallant, Y. A., & Achterberg, A. 2000, ApJ, 542, 235
Klebesadel, R. W., Strong, I. B., & Olson, R. A. 1973, ApJL, 182, L85
Kouveliotou, C., Meegan, C. A., Fishman, G. J., et al. 1993, ApJL, 413, L101
Kouveliotou, C., Woosley, S. E., Patel, S. K., et al. 2004, ApJ, 608, 872
Kulkarni, S. R., Frail, D. A., Wieringa, M. H., et al. 1998, Natur, 395, 663
Laskar, T., Berger, E., Zauderer, B. A., et al. 2013, ApJ, 776, 119
Lazzati, D., Morsony, B. J., Blackwell, C. H., & Begelman, M. C. 2012, ApJ, 750, 68
Liang, E., Zhang, B., Francisco, V., & Dai, Z. G. 2007, ApJ, 662, 1111
Livingstone, M. A., Kaspi, V. M., Gavriil, F. P., et al. 2007, Ap&SS, 308, 317
MacFadyen, A. I., Woosley, S. E., & Heger, A. 2001, ApJ, 550, 410
Malesani, D., Tagliaferri, G., Chincarini, G., et al. 2004, ApJL, 609, L5
Margutti, R., Bernardini, G., Barniol Duran, R., et al. 2011, MNRAS, 410, 1064
Margutti, R., Soderberg, A. M., Chomiuk, L., et al. 2012, ApJ, 751, 134
Margutti, R., Zaninoni, E., Bernardini, M. G., et al. 2013, MNRAS, 428, 729
Matzner, C. D., & McKee, C. F. 1999, ApJ, 510, 379
Mazzali, P. A., Deng, J., Nomoto, K., et al. 2006, Natur, 442, 1018
Mazzali, P. A., Walker, E. S., Pian, E., et al. 2013, MNRAS, 432, 2463
Melandri, A., Pian, E., Ferrero, P., et al. 2012, A&A, 547, A82
Meszaros, P., Rees, M. J., & Wijers, R. A. M. J. 1999, NewA, 4, 303
Metzger, B. D., Thompson, T. A., & Quataert, E. 2007, ApJ, 659, 561
Milisavljevic, D., Soderberg, A. M., Margutti, R., et al. 2013, ApJL, 770, L38
Nakar, E., & Sari, R. 2010, ApJ, 725, 904
Nakar, E., & Sari, R. 2012, ApJ, 747, 88
Narayan, R., Paczynski, B., & Piran, T. 1992, ApJL, 395, L83
Olivares, E. F., Greiner, J., Schady, P., et al. 2012, A&A, 539, A76
Paczynski, B. 1998, ApJL, 494, L45
Perley, D. A., Cenko, S. B., Corsi, A., et al. 2013, arXiv:1307.4401
Petrov, L., Phillips, C., Bertarini, A., Murphy, T., & Sadler, E. M. 2011, MNRAS, 414, 2528
Pian, E., Amati, L., Antonelli, L. A., et al. 2000, ApJ, 536, 778
Pian, E., Mazzali, P. A., Masetti, N., et al. 2006, Natur, 442, 1011
Sanders, N. E., Soderberg, A. M., Valenti, S., et al. 2012, ApJ, 756, 184
Sari, R., Piran, T., & Halpern, J. P. 1999, ApJL, 519, L17
Sault, R. J., Teuben, P. J., & Wright, M. C. H. 1995, in ASP Conf. Ser. 77, Astronomical Data Analysis Software and Systems IV, ed. R. A. Shaw, H. E. Payne, & J. J. E. Hayes (San Francisco, CA: ASP), 433
Sironi, L., Spitkovsky, A., & Arons, J. 2013, ApJ, 771, 54
Soderberg, A. M., Berger, E., Page, K. L., et al. 2008, Natur, 453, 469
Soderberg, A. M., Brunthaler, A., Nakar, E., Chevalier, R. A., & Bietenholz, M. F. 2010a, ApJ, 725, 922
Soderberg, A. M., Chakraborti, S., Pignata, G., et al. 2010b, Natur, 463, 513
Soderberg, A. M., Kulkarni, S. R., Berger, E., et al. 2004, Natur, 430, 648
Soderberg, A. M., Kulkarni, S. R., Nakar, E., et al. 2006a, Natur, 442, 1014
Soderberg, A. M., Nakar, E., Berger, E., & Kulkarni, S. R. 2006b, ApJ, 638, 930
Starling, R. L. C., Page, K. L., Pe'Er, A., Beardmore, A. P., & Osborne, J. P. 2012, MNRAS, 427, 2950
Starling, R. L. C., Wiersema, K., Levan, A. J., et al. 2011, MNRAS, 411, 2792
Tan, J. C., Matzner, C. D., & McKee, C. F. 2001, ApJ, 551, 946
Thompson, T. A., Chang, P., & Quataert, E. 2004, ApJ, 611, 380
Tiengo, A., Mereghetti, S., Ghisellini, G., Tavecchio, F., & Ghirlanda, G. 2004, A&A, 423, 861
Troja, E., Sakamoto, T., Guidorzi, C., et al. 2012, ApJ, 761, 50
Usov, V. V. 1992, Natur, 357, 472
Virgili, F. J., Liang, E.-W., & Zhang, B. 2009, MNRAS, 392, 91
Wang, X.-Y., Li, Z., Waxman, E., & Mészáros, P. 2007, ApJ, 664, 1026
Watson, D., Hjorth, J., Levan, A., et al. 2004, ApJL, 605, L101
Waxman, E., Mészáros, P., & Campana, S. 2007, ApJ, 667, 351
Wieringa, M., Soderberg, A., & Edwards, P. 2010, GCN, 10533, 1
Wilson, W. E., Ferris, R. H., Axtens, P., et al. 2011, MNRAS, 416, 832
Woosley, S. E. 1993, ApJ, 405, 273
Xu, D., de Ugarte Postigo, A., Leloudas, G., et al. 2013, ApJ, 776, 98
Zhang, B., Fan, Y. Z., Dyks, J., et al. 2006, ApJ, 642, 354
Zhang, B., & Mészáros, P. 2001, ApJL, 552, L35
Zhang, B., & Mészáros, P. 2004, IJMPA, 19, 2385
Zhang, B.-B., Fan, Y.-Z., Shen, R.-F., et al. 2012, ApJ, 756, 190